8 Electromagnetic induction

The electromagnetic (EM) induction method, traditionally used for mining, groundwater, and geothermal exploration and geological mapping (Grant and West, 1965; Nabighian, 1988; 1991), is growing in popularity for near-surface geophysical applications (McNeill, 1990; Nobes, 1996; Tezkan, 1999; Pellerin, 2002; Fitterman and Labson, 2005; Everett, 2012). The controlled-source variant of the method utilizes low-frequency (~ 1–100 kHz) time variations in electromagnetic fields that originate at or near the surface and diffuse into the subsurface. The ground-penetrating radar (GPR) technique is distinct from the EM induction method in the sense that the former utilizes a higher frequency range > 1 MHz for which wave propagation, rather than diffusion, is the dominant energy transport mechanism. The diffusive regime is marked by the requirement $\sigma >> \omega\varepsilon$ where σ [S/m] is electrical conductivity, ω [rad/s] is angular frequency, and ε [F/m] is dielectric permittivity. The latter plays no physical role in the EM induction method. Instead, EM induction measurements respond almost entirely to the bulk subsurface electrical conductivity and, in particular, the spatial distribution of highly conductive zones (Everett, 2005). Instrumentation is readily available, easy to use, and reliable. Electric fields are sensed by pairs of grounded electrodes, i.e.voltmeters, while time-variations of magnetic fields are most commonly sensed using induction coils.

8.1 Introduction

The electrical conductivity structure of the subsurface, as determined from EM induction measurements, can be interpreted in the context of a wide variety of potential targets and application areas, see Table 8.1. Fundamentally, EM methods respond with good sensitivity to fluid type, clay content, and porosity. An overview of the physical and chemical factors that control the bulk electrical conductivity of geomaterials is provided by Gueugen

Table 8.1 Application areas and targets of EM induction geophysics.		
Resistive targets	Intermediate targets	Conductive targets
Permafrost zones	Faults, fracture zones	Seawater intrusion
Aggregate deposits	Archaeological structures	Saline and inorganic plumes
Crystalline rock	Precision agriculture	Clay lenses, claypan soils
Caves, karst	Freshwater aquifers	Pipelines, steel drums, UXO

and Palciauskas (1995). The two case histories that follow serve as an introduction to the use of airborne and ground-based EM methods in near-surface investigations.

Example. Airborne EM mapping of a saline plume.

Soil and groundwater salinization negatively affects agriculture, water supplies, and ecosystems in arid and semi-arid regions worldwide. In Texas, especially before the 1960s and the tightening of environmental regulations, subsurface brines produced during oilfield drilling activities were frequently discharged into surface disposal pits which subsequently leaked their contents into the groundwater. Electromagnetic geophysical methods are capable of mapping conductive saline water concentrations, which are typically $\sigma \sim 0.1$–1.0 S/m, that invade geological backgrounds of $\sigma \sim 0.001$–0.01 S/m. Paine (2003) describes airborne EM mapping of such an oilfield brine plume in Texas (Figure 8.1). The plume is associated with a large area barren of vegetation that formed on a Pleistocene alluvial terrace of the Red River in the 1980s.

A helicopter EM system was employed consisting of coplanar horizontal coils and coaxial vertical coils flown at ~ 30 m altitude and operating at several frequencies between 0.9 and 56 kHz. The survey was performed with 100-m flight-line spacing and ~ 3 m along-track station spacing. A map of the 7.2 kHz apparent conductivity (Figure 8.1) clearly reveals the spatial extent of highly conductive ground. Many of the high-conductivity anomalies coincide with known brine-pit locations. The highest conductivity coincides with the barren area, which is bounded to the east by a topographic step to the Permian upland. The electromagnetic geophysical anomalies also find good spatial correlation with total dissolved solid (TDS) analyses based on sampled waters from monitoring wells distributed throughout the study area. The inferred boundary of the brine plume is marked on the map.


Example. Seawater intrusion in a coastal aquifer.

The intrusion of seawater into coastal freshwater aquifers is a serious problem in many places throughout the world. Human activities such as urbanization and the building of large-scale engineering projects such as dams can produce unintended negative effects on the hydrogeolgical conditions of coastal aquifers. Consequently it is important to develop methods that can identify the location of the freshwater–seawater interface. Electromagnetic geophysical methods offer an inexpensive and non-invasive alternative to drilling test boreholes. The electromagnetic detection of seawater is based on its high electrical conductivity relative to freshwater.

A ground-based electromagnetic geophysical survey of the Motril–Salobreña aquifer on the Mediterranean coast in southern Spain is reported by Duque *et al*. (2008). The geological setting is shown in Figure 8.2. The aquifer consists of Quaternary detrital sediments overlying Paleozoic and Mesozoic carbonates and metamorphics. As shown in the figure, a large dam is scheduled for construction along the Guadalfeo River that recharges the aquifer.
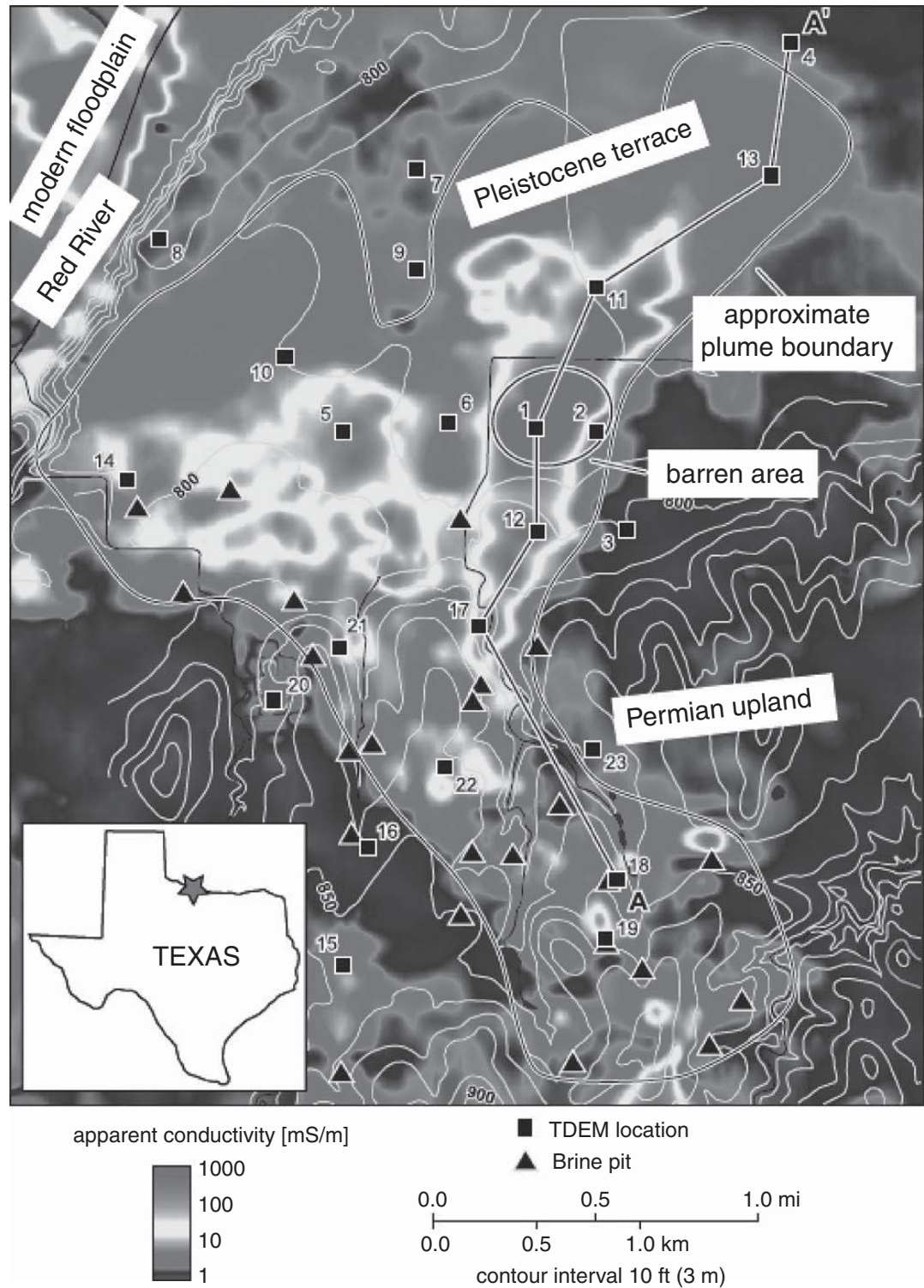
Topography and apparent resistivity at 7.2 kHz from airborne EM mapping of a north Texas oilfield brine plume. After Paine (2003).
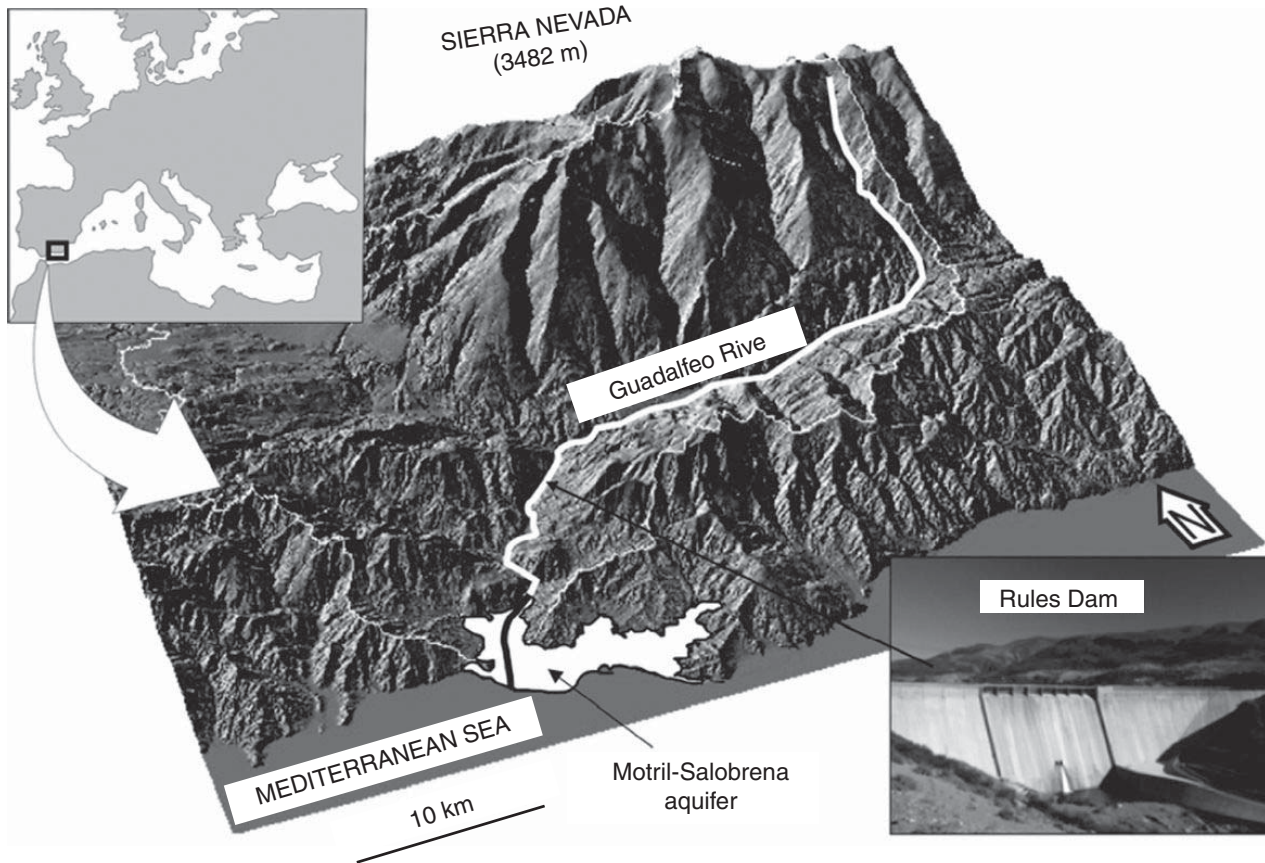
Figure 8.2 Geological setting of the Motril–Salobreña coastal aquifer (the white region) in Spain. After Duque *et al*. (2008).

The time-domain electromagnetic geophysical survey employed a central-loop config-
uration with transmitter loop sizes 50–200 m and consisted of several coast-
perpendicular transects of ~ 2 km in length with station spacing of ~ 100–200 m.
Plane-layered inversions of the measured transient responses were performed using a
commercial software package; the resulting one-dimensional (1-D) conductivity depth-
profiles were "stitched together" to form quasi-2-D depth-sections ready for interpret-
ation. Two representative interpreted depth sections appear in Figure 8.3. The interpret-
ations are based on conductivity assignments of $\sigma \sim 0.2$–2.0 S/m for seawater-saturated
sediments; $\sigma \sim 0.003$–0.2 S/m for freshwater-saturated sediments; and $\sigma < 0.003$ S/m for
the basement rocks. The location of the basement is further constrained by comple-
mentary gravity and borehole data. The results indicate that seawater intrusion into the
near-surface aquifer is minor, with the marine wedge extending not more than 500 m
inland. However, the position of the seawater–freshwater interface should be monitored
carefully in the future owing to the impending urbanization and development of this
coastal area. This case study shows that electromagnetic geophysical methods can play
an important role in determining the spatiotemporal dynamics of the seawater–
freshwater interface.
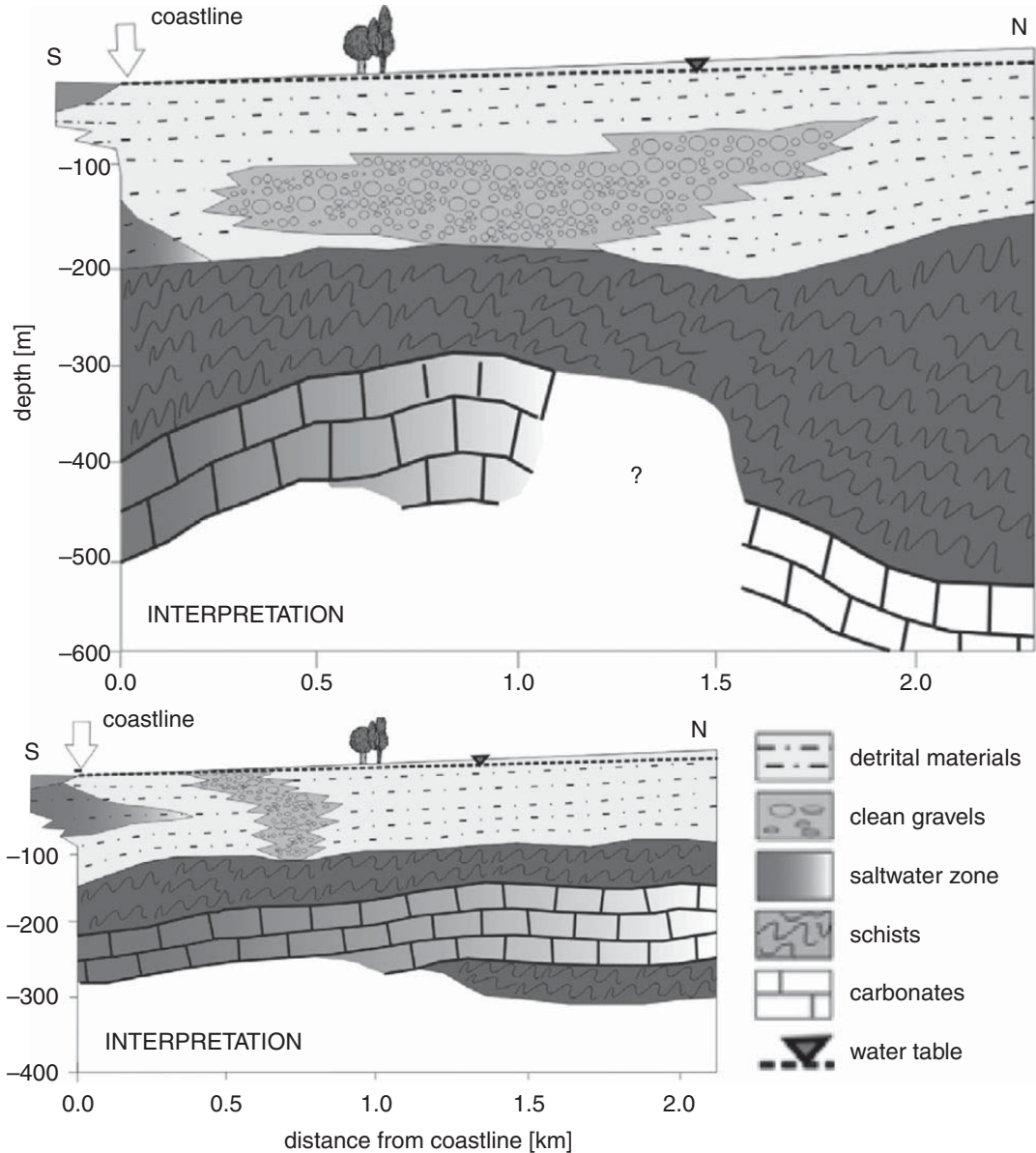
Figure 8.3 Interpretations of central-loop time-domain EM soundings in terms of seawater intrusion (red-colored areas) into the coastal Motril–Salobreña aquifer of southern Spain. After Duque *et al*. (2008).

8.2 Fundamentals

The electromagnetic geophysical method is founded on Maxwell's equations of classical electromagnetism. Standard physics textbooks such as Wangsness (1986) and Jackson (1998) are notable for their pedagogical, yet rigorous development of this topic. These texts however emphasize wave propagation rather than EM induction. The older books by Stratton (1941), Jones (1964), and Smythe (1967) treat induction in more detail and are highly recommended for advanced study. The reader is also referred to West and Macnae (1991) for a tutorial on the basic physics of induction.
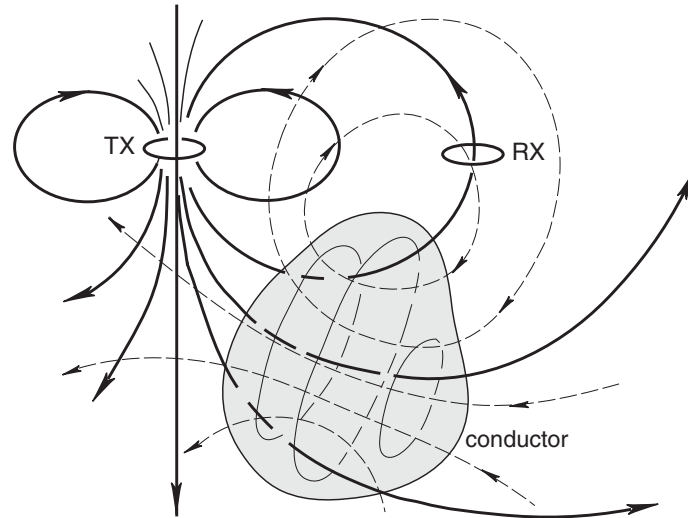
Figure 8.4   A sketch illustrating loop–loop electromagnetic target prospecting. After Grant and West (1965).

Controlled sources used by electromagnetic geophysicists may be either of the *grounded* type, as typified by the electric dipoles used in the resistivity method, or of the *inductive* type in which direct electrical contact with the ground is avoided by using an insulated wire-loop source. In the latter case, the source–ground coupling is achieved entirely by magnetic-flux linkage. The basic principles of inductive loop–loop electromagnetic prospecting for a conductive target are illustrated in Figure 8.4 and explained below.

A time-dependent electric current flowing in the transmitter (TX) coil generates a transient primary field $\mathbf{B}^P(\mathbf{r}, t)$, as shown schematically by the dark solid lines in the figure. A certain number of primary field lines flux through the conductive target, as indicated. This time-varying flux generates an electromotive force which causes eddy currents (light solid lines) of density $\mathbf{J}(\mathbf{r}, t)$ to flow in the conductor. The eddy currents, in turn, generate a secondary magnetic field $\mathbf{B}^S(\mathbf{r}, t)$, as shown by the dashed lines, that is characteristic of the target geometry, and its position and conductivity. Both primary and secondary field lines flux through the RX coil, as shown. Consequently, a voltage is induced in the RX coil containing both the primary signal from the TX and the secondary electromagnetic response of the target. Since the primary signal is known, depending only on the TX–RX configuration, it can be removed, leaving only the unknown target response.

As further aid to understand the EM method, it is worthwhile to recall that the geological medium under investigation, including a conductive target and its host, is considered to be electrically neutral. The investigated volume contains a huge number but roughly equal amounts of positive and negative charge carriers. Some of the charge carriers are mobile and may migrate or drift from place to place within the medium while other charge carriers are essentially fixed in place, bound to lattice atoms or to material interfaces. The EM induction method is concerned only with the mobile charges.

An elementary description of EM induction starts with the Lorentz force $\mathbf{F} = q(\mathbf{E} + \mathbf{v} \times \mathbf{B})$, which is experienced by a mobile charge carrier q moving with velocity $\mathbf{v}$ in an electromagnetic field $(\mathbf{E}, \mathbf{B})$. An amount of work ε is done by the electromagnetic field on the charge carrier as it completes one cycle of an arbitrary closed path L. The quantity ε is

called the electromotive force, or *emf*. The emf is not a force per se but rather a voltage or equivalently a potential. Essentially, a voltage develops along any arbitrary closed path L within a conducting body that is exposed to a time-varying **B** magnetic field. The field variations may be naturally occurring but in the controlled-source electromagnetic (CSEM) method, it is the geophysicist who shapes the external time variation with the aid of a transmitter.

The velocity **v** in the expression for the Lorentz force is interpreted as the charge-carrier *drift velocity* $\mathbf{v}_d$. Mobile charge carriers in conducting bodies migrate with an average drift velocity $\mathbf{v}_d$ in response to an applied electric field. The drift velocity satisfies $|\mathbf{v}_d| << c$, where c is the speed of light, the low velocity being due to lattice scattering of the charge carriers as they migrate. The drift velocity of electrons in standard 14-gauge copper wire carrying a 1 A current, for example, is just $|\mathbf{v}_d| \sim 40$ μm/s (Tipler, 1982). The ions of an electrolyte solution are even less mobile. The mobilities of Na^+ and Cl^- ions in seawater at temperature $T = 25$ °C are $m_+ \sim 5 \times 10^{-8}$ m^2/V s and $m_- \sim 8 \times 10^{-8}$ m^2/V s, respectively (Conway and Barradas, 1956). Since $\mathbf{v}_d = m\mathbf{E}$, this implies a very small drift velocity of $\sim 10^{-13}$ m/s in a typical electric field strength of ~ 1 mV/km.

An electric current density is associated with the drift velocity as $\mathbf{J} = nq\mathbf{v}_d$, where n is the volumetric concentration of the charge carrier. The electrical conductivity is related to the density and mobility of the charge carrier by $\sigma = nqm$ (Kittel, 1968; Gueugen and Palciauskas, 1995). Notice that an appreciable induced current does not flow in an insulator such as oil or epoxy since, in these materials, the number density n of mobile charges is negligible. It is the induced drift of mobile charges or eddy current **J**, acting as a secondary source of electromagnetic field, that generates the electromagnetic response measured by geophysicists.

In addition to the mobile charges that are present in conductive geomaterials, there certainly also exist *bound charges* that are not able to drift freely but nevertheless experience the Lorentz force **F** in the presence of an applied electromagnetic field. The motion of these bound charges leads to several types of *polarization*, foremost of which are atomic and molecular polarization, as earlier discussed in connection with the induced polarization (IP) method. Other types of bound-charge motion are also possible, but none of these are of direct relevance to the CSEM method. In other words, neither the bound charges that are confined to individual atoms, nor the mobile charges that are trapped at material interfaces, make any signficant contribution to the EM induction response. Such motions are capacitive effects; as shown in the next chapter, they are a very important aspect of the ground-penetrating radar (GPR) technique.

8.3 The skin effect

The depth of penetration of the EM induction method is limited by the efficiency of the conversion of the transmitted electromagnetic energy into kinetic energy of the mobilized subsurface charge carriers. The higher the electrical conductivity σ, the greater the efficiency and consequently the smaller the depth of penetration. The well-known *skin effect*
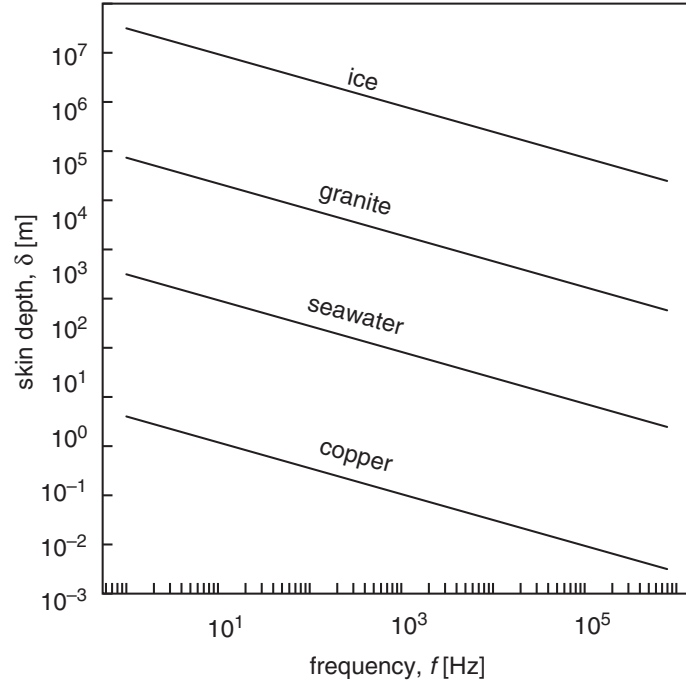
Figure 8.5   Skin depth as a function of frequency for several important non-magnetic geomaterials.

states that normally incident plane-wave signals lose $1/e \sim 0.368$ of their incident ampli-
tude after penetrating one skin depth δ into a medium of conductivity σ,

$$\delta = \sqrt{\frac{2}{\mu\sigma\omega}}, \tag{8.1}$$

where μ is magnetic permeability, $\omega = 2\omega f$ is the transmitted frequency, and $e \sim 2.71828$ is
the base of the natural logarithm, that is, $e = \exp(1)$.

   In the EM method, the magnetic permeability is almost always assumed to be equal to its
free space value, $\mu = \mu_0$, even in the presence of magnetite-bearing rock formations. An
important exception to this rule occurs if compact ferrous metal targets, such as pipelines,
steel drums, or unexploded ordnance (UXO), are being investigated (e.g. Pasion, 2007) in
which case $\mu \sim 1.05\mu_0$–$50\mu_0$, or even higher. To explore the depth of penetration in some
common non-magnetic geomaterials, typical values found in the literature for conductivity
can be used: $\sigma \sim 10^{-9}$ S/m (ice); $\sigma \sim 10^{-4}$ S/m (granite); $\sigma \sim 3.2$ S/m (seawater); and $\sigma \sim$
10^6 S/m (copper). The graphs of $\delta(f)$ for these materials appear in Figure 8.5.

   For loop-source excitation, the skin effect remains but the field distribution inside the
Earth becomes more complicated due to the compact nature of the source. The electric-
field intensity associated with diffusion from a loop source into a uniformly conducting
halfspace is shown, in the frequency domain, in Figure 8.6a. The contours are shown in a
vertical plane passing through the center of loop. Considering the azimuthal symmetry of
the problem, the electric-field intensity takes on the appearance of a toroidal "smoke ring."
The position of the maximum smoke-ring intensity in terms of the skin depth δ, as given by
Equation (8.1), is shown in Figure 8.6b.
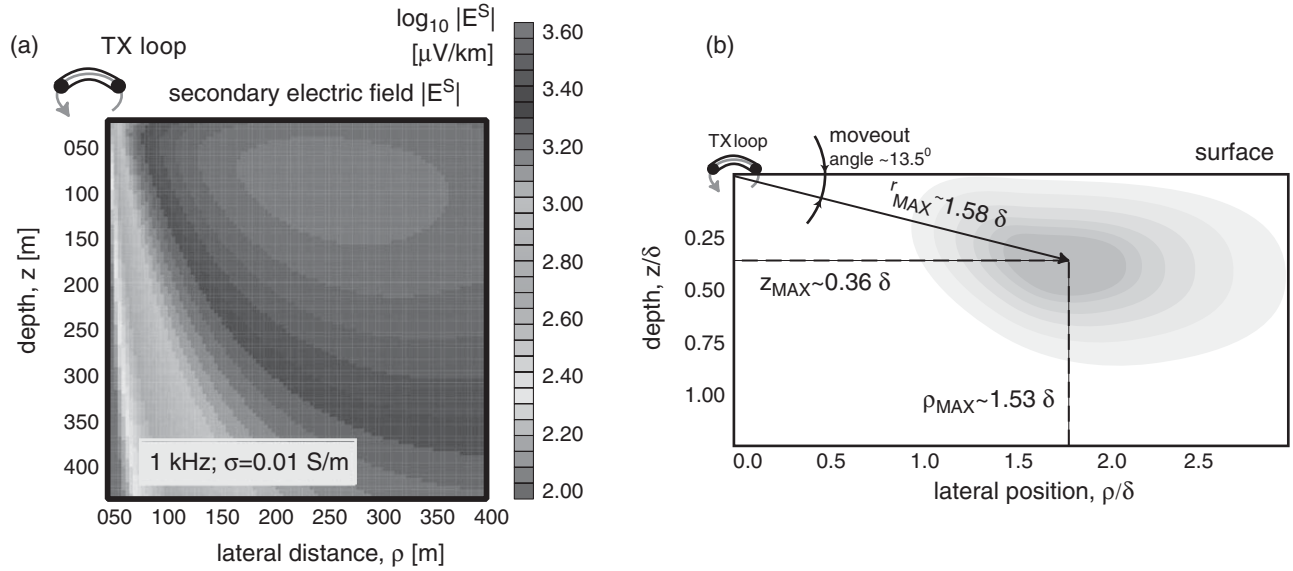
Figure 8.6 (a) Electric-field intensity due to loop excitation in a uniform halfspace; (b) position of maximum intensity of the electric field in terms of skin depth.

8.4 Inductively coupled *LR* circuits

Considerable insight into the physics of an electromagnetic geophysical prospecting system may be gained by analyzing the behavior of a roughly equivalent system of three inductively coupled *LR* circuits (Grant and West, 1965), as shown below in Figure 8.7. In the equivalent system, the TX loop is modeled as *LR* circuit 1 with resistance R_1 and self-inductance L_1. Similarly, the RX coil is modeled as circuit 2 with its own resistance and self-inductance, respectively R_2 and L_2. The conductive body, which could represent a compact target such as an ore body or a UXO, or even an entire halfspace, is modeled by circuit 3 with (R_3, L_3), as shown.

Let us first examine the primary interaction between the TX loop and the RX coil in free space without the presence of the Earth/target. The *mutual inductance* between the TX and the RX circuits is given by M_{12}. In general, given two loops i and j, the mutual inductance M_{ij} is defined as the magnetic flux that passes through loop j due to a unit electric current flowing in loop i. Thus, mutual inductance is purely a geometric parameter that depends on the relative orientation and location of the two loops with respect to each other. Notice also that $M_{ij} = M_{ji}$. The *self-inductance* L_i is the magnetic flux that passes through loop i caused by unit current flow in the same loop, hence, $L_i = M_{ii}$.

Suppose Φ_j is the magnetic flux through loop j, defined according to

$$\Phi_j = \int_A \mathbf{B}_j \cdot \hat{\mathbf{n}} dA, \qquad (8.2)$$